Digest Journal of Nanomaterials and Biostructures Vol. 20, No. 4, October-December 2025, p. 1557-1569

Electrical optimization of metal/GaN/GaAs structures: role of GaN thickness, contact metal, and frequency

N. Zougagh [a,c,*], A. Guen [a,d], Z. Benamara [b,c], H. Mazari [b,c], G. Monier [e], C. Robert-Goumet [e]

[a] *University Abou-Bekr Belkaid of Tlemcen, Faculty of Technology GEE. Departement Tlemcen13000, Algéria.*
[b] *Universiy Djillali Liabès of Sidi bel abbés 22000, Algéria.*
[c] *Applied Microelectronics Laboratory Sidi bel abbés 22000, Algéria.*
[d] *Research Unit for Materials and Renewable Energy URMER. Tlemcen13000, Algéria.*
[e] *Institut Pascal, University Clermont Auvergne, Blaise Pascal F-63000 Clermont-Ferrand, France.*

This study aims to optimize a metal/gallium nitride (GaN)/ gallium arsenide (GaAs) heterostructure and this will be done by varying several parameters. More specifically, this work allows the investigate of influence of GaN thin-film thickness on the I–V and C-V characteristics of an Hg/GaN/GaAs structure. The effect of the Schottky contact in two different metal configurations (Au/GaN/GaAs and Hg/GaN/GaAs) has also been evaluated. Finally, the influence of frequency variation on the capacitance-voltage C-V and conductance-voltage (G-V) characteristics of the Au/GaN/GaAs structure has been assessed. In this work, GaN thin films were grown on four GaAs substrates, which were labeled A1, A2, A4, and A3, with respective thicknesses of: 1.8 nm, 2.8 nm, 2.4 nm, and 22 nm. Increasing the GaN layer thickness for the three structures A1, A2, and A3 improved the current conduction and notably reduced the interfacial layer, thereby enhancing electron tunneling and leading to a dominant tunnel current. The extracted Schottky barrier heights were respectively 0.80 V, 0.74 V, and 0.60 V for A1, A2, and A3 samples. The corresponding series resistances measured were respectively 86 Ω, 66 Ω, and 45 Ω. From the $1/C^2$-V plots, the diffusion voltages obtained were 0.55 V, 0.70 V, and 4 V for A1, A2, and A3, respectively. Replacing mercury in the Hg/GaN/GaAs structure (A4) with gold to form a new structure that is Au/GaN/GaAs markedly improved the structure's performance. The ideality factor and also the series resistance decreased, while the doping concentration remained nearly constant at $1.5 \times 10^{16}/cm^3$. The ideality factors were found to be 1.8 for Au/GaN/GaAs and 2.9 for Hg/GaN/GaAs, whereas the series resistances were 44 Ω and 104 Ω for Au/GaN/GaAs and Hg/GaN/GaAs, respectively. Conductance-voltage G-V and capacitance-voltage C-V measurements at three different frequencies that are 10 kHz, 100 kHz, and 1 MHz for the Au/GaN/GaAs structure studied revealed that the device behaves like a metal-insulator-semiconductor (MIS) structure at low frequencies and like a Schottky diode at high frequencies.

(Received: 30 September 2025; Accepted: 10 December 2025)

Keywords: GaN/GaAs, nitriding, hetero-structure, Schottky, Hg, Au, Characterization, Tunnel current, Frequency1

1. Introduction

Silicon technology is limited by its intrinsic properties. Accordingly, the design of increasingly efficient electronic devices has required the use of non-silicon semiconductors, predominantly those with high carrier mobility, wide bandgap, and direct band transitions structures. Among these, III–V semiconductors are considered ideal candidates for device optimization due to their exceptional physical properties, making them suitable not only for

* Corresponding author: zougagh1893@yahoo.fr
https://doi.org/10.15251/DJNB.2025.204.1557

microwave and power electronic applications but also for low-power optoelectronic devices such as photoluminescent and laser diodes [1]. Nitriding III–V semiconductors of the gallium arsenide (GaAs) type enables the development of gallium nitride (GaN)/GaAs structures and the growth of heterostructures with GaN nanofilms of varying thicknesses on GaAs substrates. This process removes a large portion of the native oxide present on the GaAs surface and reduces leakage currents, given that GaN is a chemically stable semiconductor. In this work, we focused on the growth of GaN layers using a high-voltage discharge source under ultra-high vacuum conditions. This method allowed the formation of heterostructures consisting of GaN nanofilms of different thicknesses deposited on GaAs substrates. At the end of this work, the structure was optimized by varying the metal used for the Schottky contact and comparing the performance of two configurations: Au/GaN/GaAs and Hg/GaN/GaAs. Finally, the capacitance-voltage behavior of the Au/GaN/GaAs structure was investigated as a function of frequency.

2. Experimental study

Nitriding GaAs enables the fabrication of GaN/GaAs structures, resulting in heterostructures with GaN nanofilms exhibiting a range of thicknesses on GaAs substrates. This process consists of subjecting the GaAs substrate to a stream of active nitrogen that is generated by a high-voltage plasma source under ultra-high vacuum conditions. Spectroscopic analyses, including Auger electron spectroscopy (AES) and X-ray photoelectron spectroscopy (XPS), revealed insights into the internal structure of the devices as well as their physical properties. Electrical characterization through current-voltage and capacitance-voltage measurements also yielded meaningful informations about the GaN/GaAs heterostructures. To improve the quality of the ohmic contact, in was deposited on the backside of the structures using N_4Cl. The assembly was thereafter heated to 350 °C for 5 minutes to allow the in to diffuse into the GaAs. In the first step, the A4 structure was metallized with a mercury pad to create a temporary contact with a surface area of 7.85 × 10^{-3} cm2, forming the Hg/GaN/GaAs structure. After removing and cleaning the temporary mercury contact via thermal evaporation, the front side of the A4 structure was metallized with gold generating a permanent contact of roughly 2 × 10^{-3} cm^2, resulting in an Au/GaN/GaAs structure.

The technological steps for nitriding to create different thicknesses of GaN on GaAs are summarized in Table 1.

	A_1	A_2	A_3	A_4
Concentration of GaAs per cubic centimeter cm^{-3}	$(5 \pm 0.1)\times10^{15}$	$(5 \pm 0.1)\times10^{15}$	$(1.5 \pm 0.1)\times10^{18}$	$(5 \pm 0.1)\times10^{15}$
Nitriding condition	300 °C/20 min	300 °C/1 h	550 °C /3 h	300 °C/1 h
Annealing	300 °C/1 h	400 °C / 1 h	550–600 °C /2 h	No Annealing
GaN layer thickness	1.8 nm	2.8 nm	22 nm	2.4 nm
Schottky contact	Hg	Hg	Hg	~~Hg~~ → Or
Ohmic contact	Sn+N_4Cl	Sn+N_4Cl	Sn+N_4Cl	Sn+N_4Cl

Table 1. Technological stages for structures A1, A2, A3, and A4.

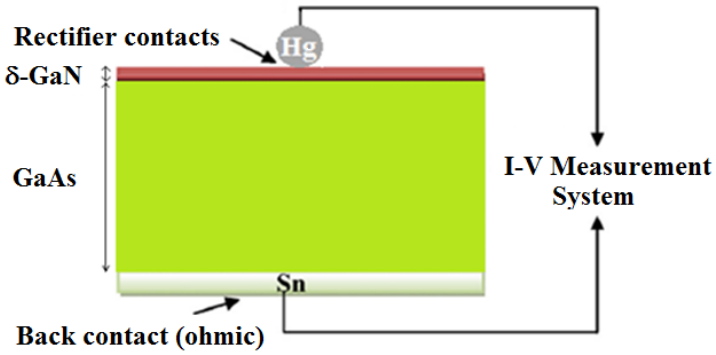

Fig. 1. Diagram of the Hg/GaN/GaAS structure.

To study the effect of GaN on GaAs substrates, current-voltage I–V measurements were conducted on our three samples, which are A1, A2, and A3, each having different GaN thicknesses. These experiments were performed using a semiconductor parameter analyzer that is an HP 4155B.

3. Experimental Results and Discussion

3.1 Optimizing Hg/GaN/GaAs Structures via GaN Layer Thickness Electrical current-voltage characteristics and modeling

The experimental I–V characteristics under forward bias can be interpreted using the thermionic emission model, which is described by the following expression:[2]

$$I = I_{TE0} \times \exp\left(\frac{q(V - R_S I)}{nkT}\right) - I_{TE0} \quad (1)$$

$$I_{TE0} = S.A.T^2 \exp(-\chi^{0,5} \times \delta) \exp\left(\frac{q\phi_{bn}}{kT}\right) \quad (2)$$

Where:

I_{TE0} represents the saturation thermionic current.

Rs is the series resistance;

S is the contact area;

q is the electron charge;

T is the temperature;

A is an effective Richardson constant,

δ is the thickness of the interfacial layer,

χ is the average barrier height present in the interface layer.

k is the Boltzmann constant,

ϕ_{bn} is the effective barrier height. It is expressed as [3]:

$$\phi_{bn} = \frac{kT}{q} \ln\left(\frac{S.A.T^2}{I_{TE0}}\right) \quad (3)$$

The ideality factor noted “n” is directly extracted from the slope of the forward-biased I-V curve’s linear region and expressed as follows:[4]

$$n=\frac{q}{kT}\left(\frac{\partial V}{\partial \ln(I)}\right) \quad (4)$$

The I–V curves of the three samples presented clearly exhibit the behavior of a rectifying, or Schottky, contact. The I–V curves that we obtained for A1, A2, and A3 samples are given in Figure 2, measured at a temperature of 300 K. The saturation current, barrier height, ideality factor, and series resistance were extracted from the I−V characteristics and summarized in Table 2.

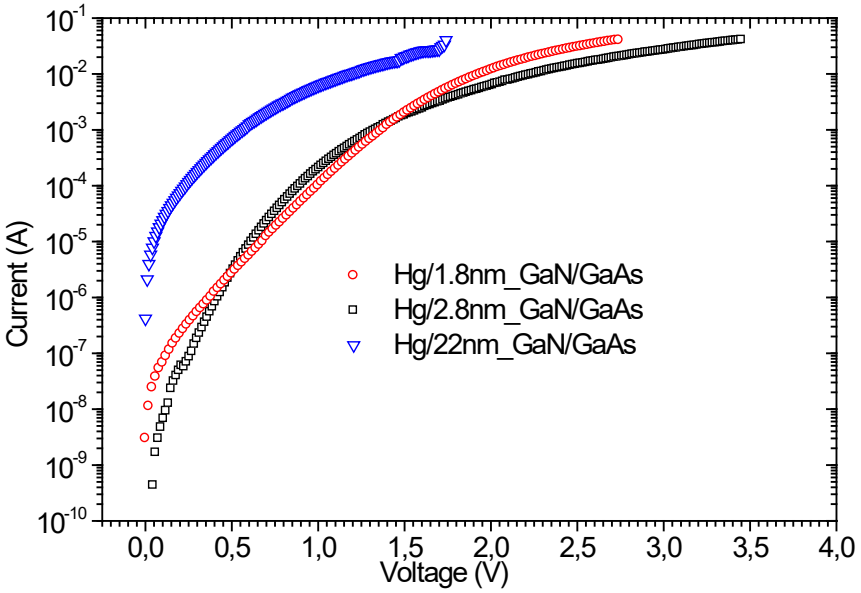

Fig. 2. Experimental I−V characteristics of samples A_1, A_2, and A_3.

Table 2. Extraction of I (V) parameters.

Samples	I_s (A)	n	R_s (Ω)	Φ_{Bn} (V)
A_1	4.1×10^{-10}	1.5	86	0.80
A_2	5.6×10^{-9}	1.87	66	0.74
A_3	5.7×10^{-7}	1.3	45	0.6

Our results are consistent with those that have been reported by M. Ambrico *et al.* [5] and by Mehmet Ali Ebeoglu [6]. These results show an ideality factor greater than 1; this has also been observed in other structures containing SiC and GaN [7]. This indicates that additional transport mechanisms contribute to the total current (Eq. 5). In addition to the thermionic current ITE, contributions arise from the generation-recombination current IGR, the leakage current ILK, and particularly the tunneling current ITU.

$$I_{tot} = I_{TE} + I_{GR} + I_{TU} + I_{LK} \quad (5)$$

$$I_{tot} = I_{TE0}\left(\mathrm{Exp}\left(\frac{q(V-R_sI)}{kT}\right)-1\right)+I_{GR0}\left(\mathrm{Exp}\left(\frac{q(V-R_sI)}{2kT}\right)-1\right) + I_{TU0}\left(\mathrm{Exp}\left(\frac{q(V-R_sI)}{E_0}\right)-1\right)+\frac{(V-R_sI)}{R_P} \quad (6)$$

Where ITE0, IGR0, and ITU0 are zero-bias components, and E0 is a particular parameter suggested by Padovani and Stratton [8] that indicates the barrier transparency.

With: $E_0 = E_{00} \coth\left(\frac{E_{00}}{kT}\right)$ (7)

$$E_{00} = \frac{qh}{4\pi}\sqrt{\frac{N_D}{\varepsilon_S m_n^*}} \quad (8)$$

Rp is the shunt resistance, and ε_s is the semiconductor permittivity.

Figures 3, 4, and 5 shows the effect of the generation-recombination current, leakage current, and tunneling current on the final relationship. The parameters chosen for a data fit at 300 °C are presented in the table 3.

Table3. Parameters Selected for Simulating I-V Curve.

Samples	A_1	A_2	A_3
Nd (cm^{-3})	$(5 \pm 0.1)\times10^{15}$	$(5 \pm 0.1)\times10^{15}$	$(1.5 \pm 0.1)\times10^{18}$
Richardson constant A* (A cm^{-2} K^{-2}) [9]	26.4	26.4	26.4
Effective electron mass m_n^*[9]	22×10^{-2} m_0	22×10^{-2} m_0	22×10^{-2} m_0
Rs (ohms) (introduced)	170 → I_{GR} 700 → I_{TU} 75 → I_{TE}	250 → I_{GR} 96 → I_{TU} 40 → I_{TE}	85 → I_{GR} 75 → I_{TU} 60 → I_{TE}
Rp (ohms) (introduced)	5×10^7	5×10^6	5×10^3
E_0 (meV) (introduced)	75	126	90
I_{GR0} (A) (introduced	7×10^{-15}	4×10^{-18}	2×10^{-11}
I_{TU0} (A) (introduced)	2×10^{-9}	3.25×10^{-8}	4.5×10^{-6}
I_{TE0} (A) (introduced)	1×10^{-22}	2.4×10^{-21}	2.0×10^{-22}

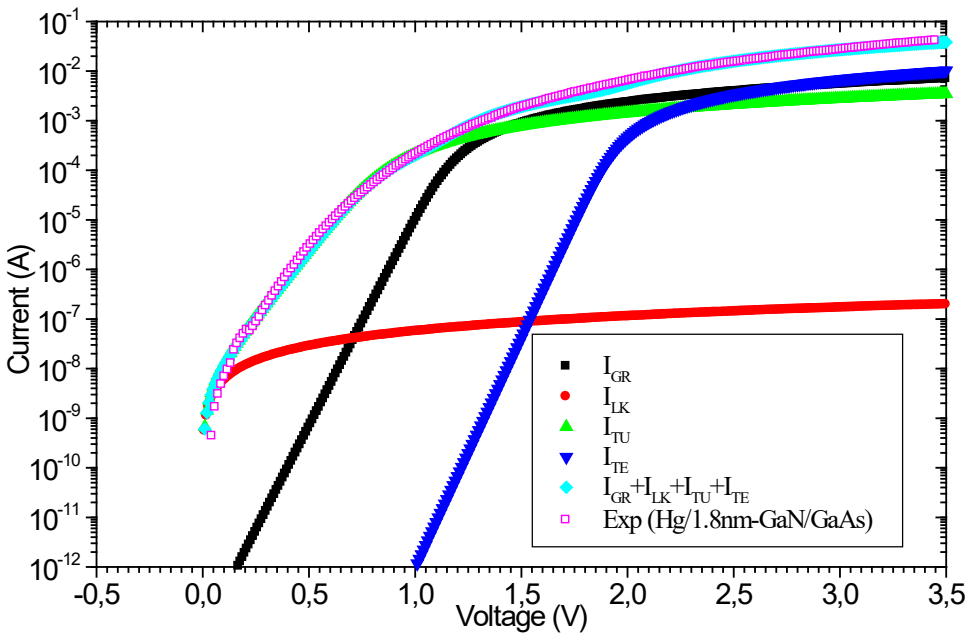

Fig.3. Measured and theoretical I−V characteristics for A1 structure.

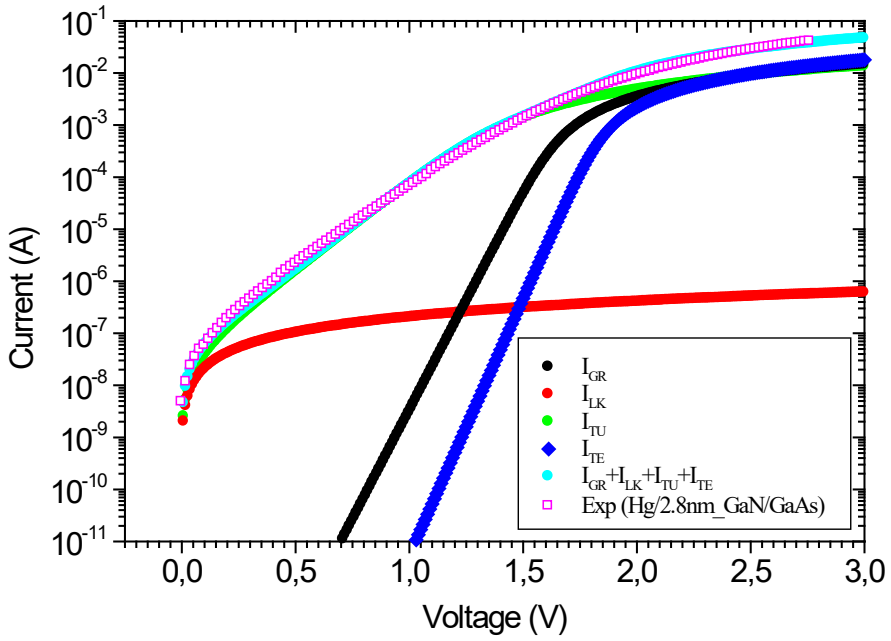

Fig.4. Experimental and theoretical I–V characteristics of A2 structure.

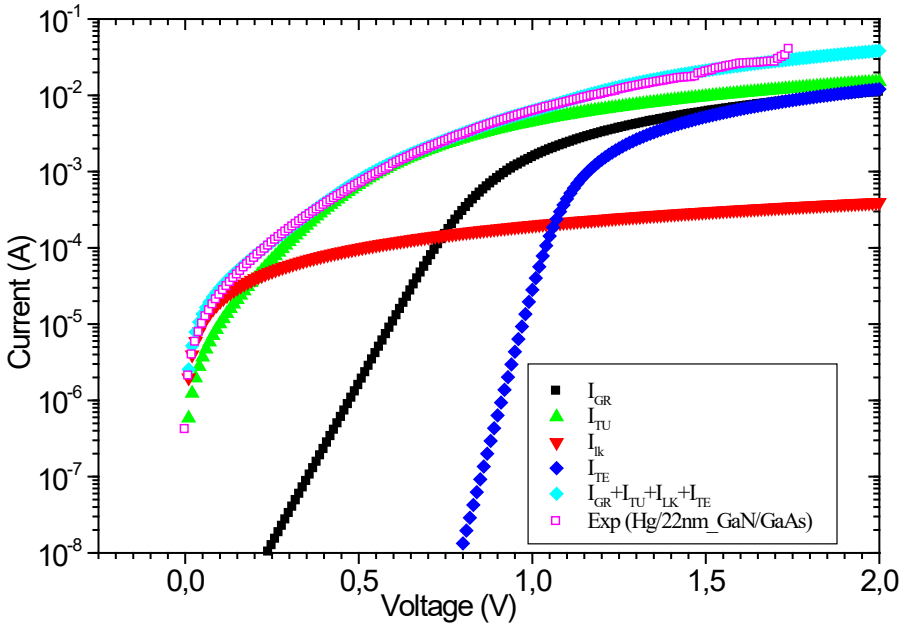

Fig. 5. Meseared and theoretical I–V characteristics for A3 structure.

It is evident that the tunneling current dominates in the three structures studied, particularly at low voltages, while the other currents become significant only at higher voltages.

a. Electrical capacitance-voltage characterization

The C-V measurements were performed using the KEITHLEY Test System 590 CV Analyzer, with a DC voltage range from −4 V to 0 V at 1 MHz. The inverse square of the capacitance was plotted as a function of voltage for the three samples (Fig. 6).

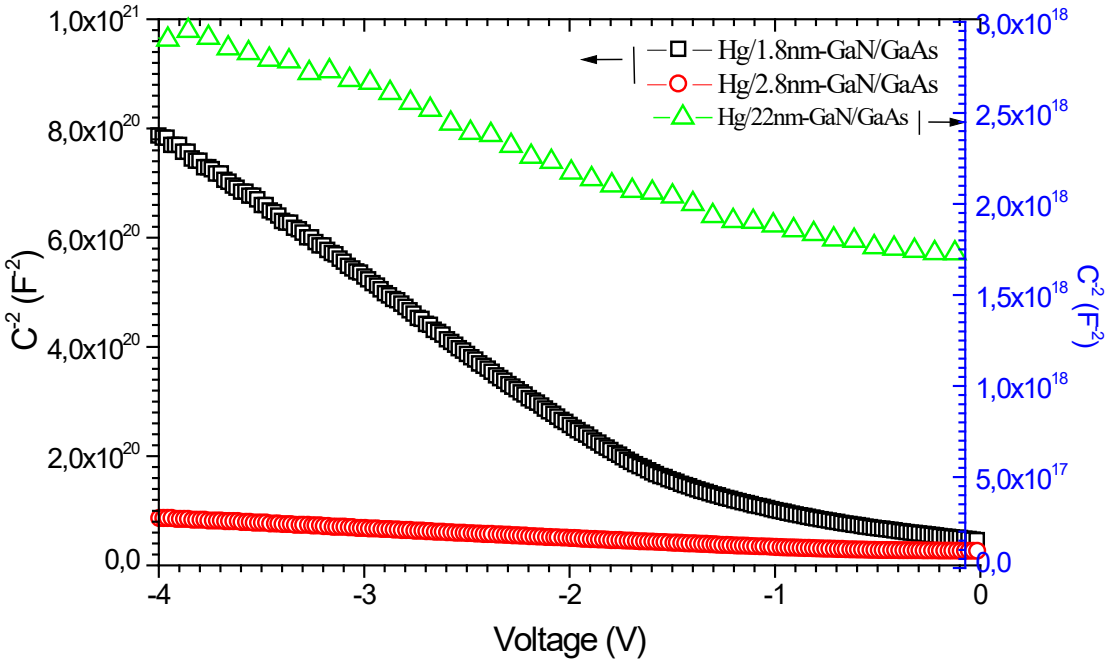

Fig. 6. Inverse plot of capacitance versus bias voltage.

A moderately thick GaN layer gives rise to the accumulation of a residual positive electric charge in the Hg/GaN/GaAs structure (Figure 6). This charge is confined within the GaN layer, and its magnitude depends on the thickness of the layer [10].

The change in the slope of the curve is directly related to the doping profile (Figure 6) and can be expressed as: [11].

$$N_{C\text{-}V} = \frac{-2}{q\varepsilon_r\varepsilon_0} \cdot \frac{1}{d\left(1/C_{SC}{}^2\right)/dV} \tag{9}$$

$$W = \sqrt{\frac{2\varepsilon_r\varepsilon_0}{qN_d}\left(|V_d| - \frac{kT}{q}\right)} \tag{10}$$

ε_0: vacuum permittivity

ε_r: the relative permittivity of the GaN layer, which is equal to $9.5\varepsilon_0$ [12].

The built-in potentials obtained from the $1/C^2$ versus voltage plot for the three samples are 0.7 V for A2, 0.55 V for A1, and approximately 4 V for A3. It is noted that the built-in potential for sample A3 is significantly higher. This is due to the residual capacitance located in the GaN layer of this structure, as demonstrated by K. Ameur *et al*. [10].

The figure 7 shows the variation of the doping profile of each structure as a function of the space-charge region thickness.

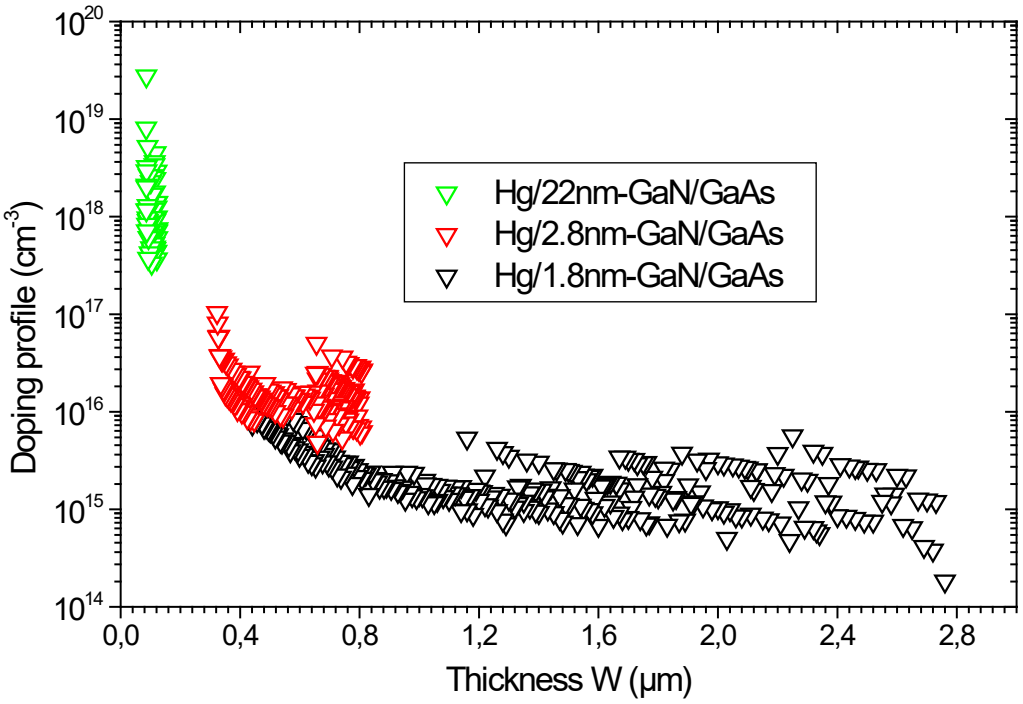

Fig. 7. Doping concentration as a function of the variation in the space-charge region for the three samples.

According to the results we obtained and represented in the figure above, unintentional dopant migration from the GaAs substrate toward the GaN layer is evident. The dopant concentration in the interfacial layer depends not only on the initial doping level of the substrate but also on the GaN layer thickness. In other words, dopant migration is limited when the GaN layer provides insufficient space. This behavior is noticeable in samples A1 and A2, which have identical substrate characteristics. However, dopant migration is more pronounced in sample A1 than in sample A2, due to the greater thickness of the GaN layer in A1 (2.8 nm) compared with A2 (1.8 nm).

Another plausible hypothesis, proposed by P. Perlin *et al*. [13], attributes the increase in doping concentration primarily to the intrinsic properties of GaN semiconductor that typically contains defects and residual impurities formed during growth, which introduce energy levels within the conduction band and also generate intrinsic free electrons. Consequently, GaN generally exhibits residual n-type conductivity, with electron concentrations ranging from 1017 cm^{-3} to 1020 cm^{-3} in bulk samples, and on the order of 1017 cm^{-3} in thin films grown by MOCVD or MBE.

It is also manifest that considerable dopant migration or an increase in the intrinsic concentration of GaN leads to a reduction in the thickness of the interfacial layer, thereby promoting tunneling current conduction in the Hg/GaN/GaAs heterojunction. Sample A3 confirms these evidences. In this sample, both the initial doping of the GaAs substrate and the GaN layer thickness were increased, resulting in improved current conduction and a substantial reduction of the interfacial layer thickness (Fig. 7).

The decrease in interfacial layer thickness in such structures exponentially enhances electron tunneling, making the tunneling current the dominant conduction mechanism.

3.2. Comparison between Au/GaN/GaAs and Hg/GaN/GaAs metal-semiconductor structures

a. Current-voltage characteristics

To investigate the effect of the Schottky contact in the Hg/GaN/GaAs and Au/GaN/GaAs structures considered, I–V measurements were performed and are shown in Figure 8 at a temperature of 300 °C. The saturation current, barrier height, ideality factor, and series resistance were extracted from the I–V characteristics and are summarized in Table 4.

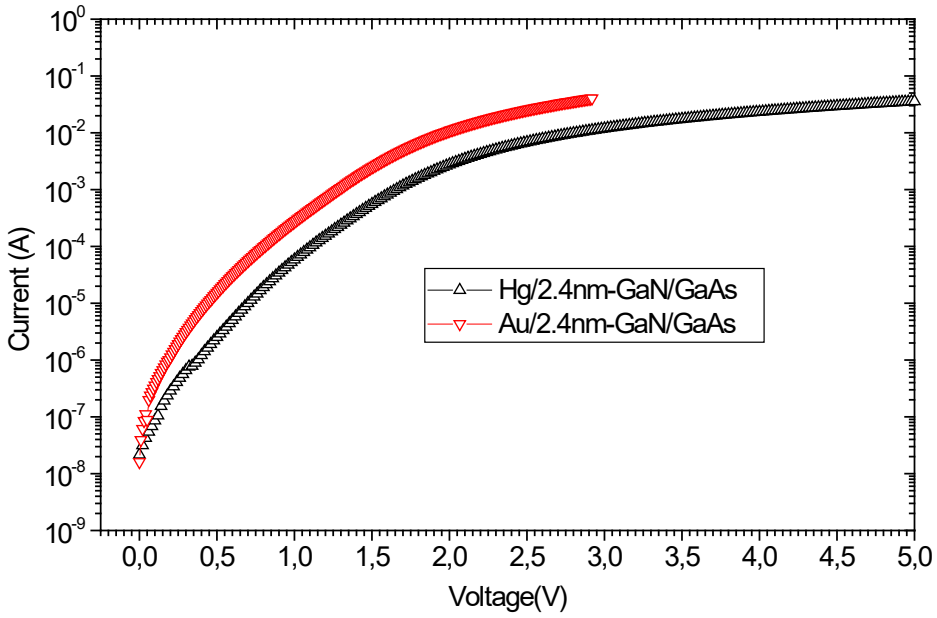

Fig. 8. Extraction and Comparison of I–V Parameters for Hg/GaN/GaAs and Au/GaN/GaAs Structures.

It is clearly observed that the Schottky contact with gold has improved the performance of the Au/GaN/GaAs structure, where the ideality factor and the series resistance have decreased compared to the Hg/GaN/GaAs structure (see Tab.5). Our results are similar to those reported by R. Khelifi, H. Mazari *et al*. [14] .

Table 5. Extraction and comparison of the I–V parameters for the two structures with different metals.

Samples	I_s (A)	n	R_s (Ω)	Φ_{Bn} (V)
Hg/2.4 nm_GaN/GaAs	3.38×10^{-8}	2.9	104	0.7
Au/2.4 nm_GaN/GaAs	2.1×10^{-8}	1.8	44	0.64

b. Electrical capacitance-voltage characterization

C–V measurements were carried out for both the Hg/GaN/GaAs and Au/GaN/GaAs structures over a voltage range of −6 V to 0 V at 1 MHz. The inverse square of the capacitance as a function of voltage for both structures is presented in Figure 9.

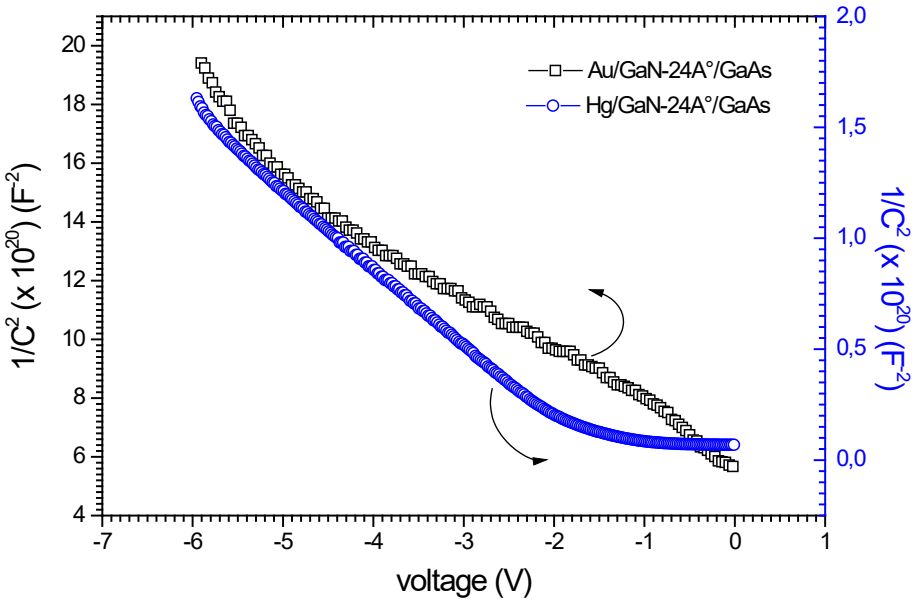

Fig. 9. 1/C². characteristic as a function of the applied voltage.

Our results indicate that the doping concentration in the Au/GaN/GaAs structure is circa $1.5 \times 10^{16}/cm^3$ and remains approximately constant over the voltage range of −6 V to 0 V. In contrast, the doping in the Hg/GaN/GaAs structure is irregular, exhibiting two distinct regions: a doping concentration of 8.36×1016 cm^{-3} between −1.5 V and −0.02 V, and $6.18 \times 1015\ cm^{-3}$ between −6 V and −3 V.

A shift is also observed in the C–V characteristic of the Hg/n-GaN/GaAs structure compared to the Au/n-GaN/GaAs structure, likely resulting from residual capacitance associated with the Hg contact, as previously reported for Hg/GaN/GaAs structure [11].

3.3. Frequency dependence of Au/GaN/GaAs structure

Capacitance-voltage (C-V) and conductance-voltage (G-V) measurements were conducted as a function of frequency for the Au/GaN/GaAs structure, which features a 2.4 nm-thick GaN layer. The C-V characteristics of this sample, measured at three frequencies (10 kHz, 100 kHz, and 1 MHz), are presented in Figures 10 and 11.

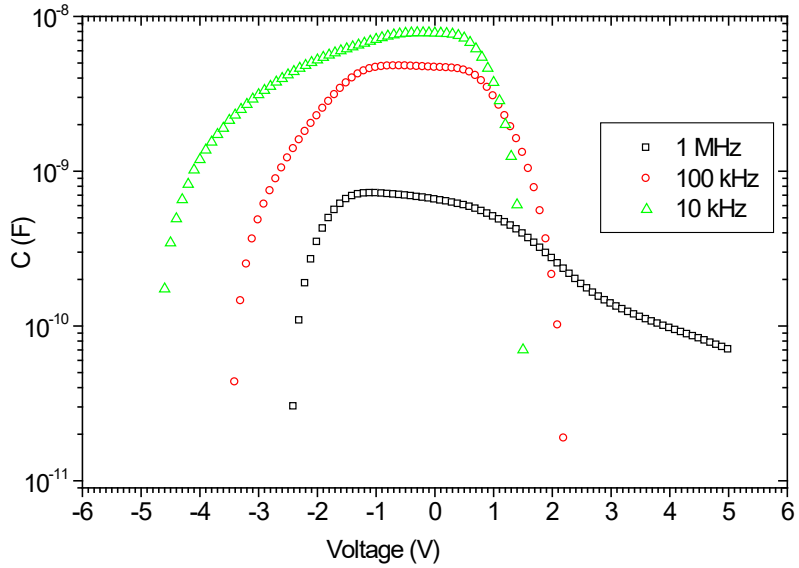

Fig. 10. C-V Characteristic at Different Frequencies of the Au/GaN/GaAs Structure

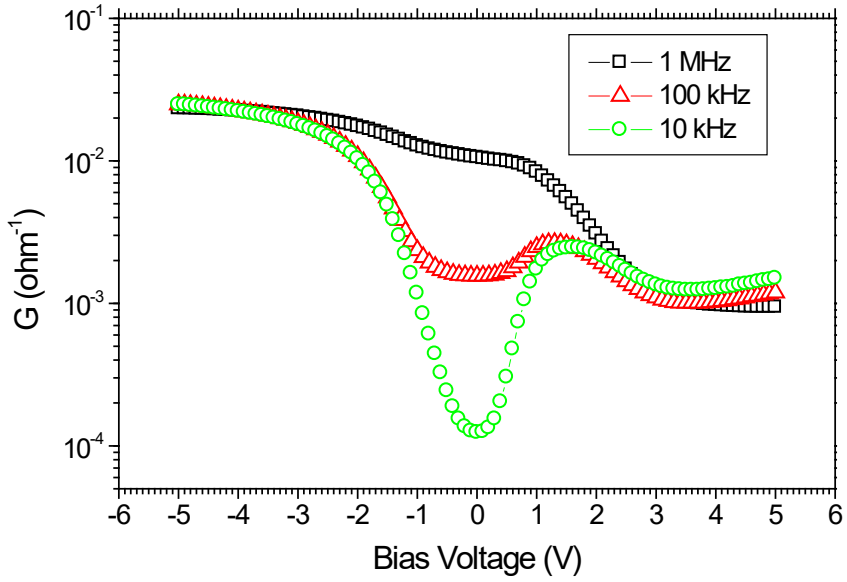

Fig. 11. G-V Characteristic at Different Frequencies of the Au/GaN/GaAs Structure.

T
he C-V characteristics, plotted at different frequencies for the Au/GaN/GaAs structure, clearly show that this structure behaves like a MIS device, with three distinguishable regions: a weak inversion region, a depletion region, and an accumulation region.

The frequency-dependent C-V characteristics of the Au/GaN/GaAs structure studied expose a pronounced depletion region along with an enhancement in capacitance at low frequencies. This additional capacitance can be attributed to the presence of interface states at the Au/GaN and/or GaN/GaAs interfaces, and may also result from trap states within the material, either in the bulk of GaN or GaAs. At high frequencies (1 MHz in our case), the alternating signal varies at a higher rate than the response time of the interface states, effectively minimizing their contribution to the total capacitance. This behavior is consistent with the findings reported by Fanash [15].

The G-V curves shown in Figure 10 indicate that the conductance values depend on frequency, particularly in the depletion region. The conductance values increase as the frequency decreases. This can be explained by the distribution of interface states and traps, which can more easily follow the alternating signal at low frequencies.

At a low frequency, in our case 10 kHz, the conductance value decreases to $1.3 \times 10^{-4}\ \Omega^{-1}$. This value reaches $10^{-2}\ \Omega^{-1}$ at 1 MHz.

4. Conclusion

In our work, comprehensive analyses of two studied structures that are Hg/GaN/GaAs and Au/GaN/GaAshave been achieved. Our analyses reveal the characteristic behavior of Schottky contacts, where tunneling dominates charge transport at low voltages. This behavior arises predominantly from an evident reduction in the interfacial layer, associated with both the unintentional migration of dopants from the GaAs substrate and the increased thickness of the GaN film. Among the examined samples, the third sample A3 illustrates most notably this correlation, exhibiting a higher diffusion voltage and a marked enhancement in conduction current.

Intrinsic defects and residual impurities within GaN additionally contribute to the generation of free carriers, thereby reinforcing the material's intrinsic n-type conductivity.

Accordingly, careful optimization of the initial doping level and GaN layer growth conditions proves essential for precise control of charge transport mechanisms in these heterojunctions.

Compared with the mercury-based contact, the Au/GaN/GaAs structure demonstrates superior electrical stability, as demonstrated by the improved current–voltage and capacitance–voltage characteristics. Enhanced parameters, such as a reduced ideality factor and lower series resistance, further corroborate its superior performance. The C-V and G-V analyses also show a clear frequency dependence: at low frequencies, the structure reveals a typical MIS behavior, where interface states and traps introduce additional capacitance and limit conductance; at high frequencies, these effects lessen, and the device exhibits a Schottky-like response with considerably improved conductance.

These results obtained in this work emphasize the critical role of frequency selection in analyzing and optimizing the performance of such structures, principally in reducing parasitic effects associated with interface states.

Moreover, these results demonstrate that metal choice, interlayer thickness, doping concentration, and operating frequency constitute a set of key parameters governing the behavior of GaN-based devices.

In general, these results open promising perspectives for the design of engineered tunnel junctions and the progress of high-performance components developed for power and high-frequency electronic applications.

Availability of Data and Materials

HEWLETT PACKARD 4155B semiconductor parameter analyzer
KEITHLEY test system. 590 CV Analyser
Auger electron spectroscopy (AES)
X-ray photoelectron spectroscopy (XPS)

Author Contributions

N. Zougagh, A. Guen, Z. Benamara, H. Mazari, G. Monier

Acknowledgements

We would like to express our gratitude to all those who helped us in any way during the writing of this manuscript.

Funding

Applied Microelectronics Laboratory, University Sidi bel abbés-Algéria.
Institut Pascal, University Clermont Auvergne, Blaise Pascal Clermont-Ferrand-France.

Conflict of Interest

The authors declare no conflict of interest

References

[1] Tachibana, H., Ishido, T., Ogawa, M., Funato, M., Fujita, S., Fujita, S. (1999), Journal of Crystal Growth, 196(1), 41–46. https://doi.org/10.1016/S0022-0248(98)00818-5
[2] H. C. Card, E. H. Rhoderick J. Appl. Phyus. D 4, 1971. doi:10.1088/0022-3727/4/10/319
[3] S.M. Sze, Physics of Semiconductor Devices, second ed., Wiley, New York, p. 245, 1981 https://download.e-bookshelf.de/download/0000/5685/22/L-G-0000568522-0015227363.pdf

[4] Arslan, E, Altındal, Ş, Özçelik, S., Ozbay, E., Semiconductor science and technology, 24 (7), (2009) http://dx.doi.org/10.1088/0268-1242/24/7/075003
[5] Ambrico, M., Losurdo, M., Capezzuto, P., Bruno, G., Ligonzo, T., Schiavulli, L., Farella, I., Augelli, V. (2005), Solid-State Electronics, 49(3), 413–419. https://doi.org/10.1016/j.sse.2004.11.007
[6] Ebeoğlu, M. A. (2008). PhysicaB: CondensedMatter, 403(1), 61–66. https://doi.org/10.1016/j.physb.2007.08.008
[7] Benmaza, H., Akkal, B., Abid, H., Bluet, J. M., Anani, M., Bensaad, Z. (2008), Microelectronics journal, 39(1), 80–84. https://doi.org/10.1016/j.mejo.2007.10.018
[8] Padovani, F. A., Stratton, R. (1966). Solid-State Electronics, 9(7), 695–707. https://doi.org/10.1016/0038-1101(66)90097-9
[9] A.Vapaille, R. Castagne, Dispositifs et circuits intégrés semi-conducteurs. Edition DUNOD, (1990). ISBN 2-04-019714-1
[10] Ameur, K., Mazari, H., Tizi, S., Khelifi, R., Benamara, Z., Benseddik, N., A, Chaib., N, Zougagh., M, Mostefaoui., L, Bideux., G, Monier., B, Gruzza., Robert-Goumet, C. (2011), Sensor Letters, 9(6), 2268-2271. https://doi.org/10.1166/sl.2011.1802
[11] M. Charfeddine., M. Gassoumi., H. Mosbahi., C. Gaquiére., M. A. Zaidi., H. Maaref. Journal of Modern Physics. 2, 1231 (2011).
[12] R. Hull, R. M. Osgood, Jr, J. Parisi, and H. Warlimont, Gallium Nitride Electronics, Springer Series in Materials Science 21, 96 (2008). https://www.scribd.com/document/367174303/Dilute-III-V-Nitride-Semiconductors-and-Material-Systems
[13] P. Perlin, T. Suski, H. Teisseyre, M. Leszczynski, I. Grzegory, J. Jun, S. Porowski, P. Bogusiawski, J. Bernholc, and J. Chervin, Towards the identication of the dominant donor in GaN, Physical review letters, 75(2), 296 (1995). doi: 10.1103/PhysRevLett.75.296
[14] Khelifi, R., MazariH., Mansouri, S., Ameur, K., Benamara, Z., Mostefaoui, M., Benseddik, N., Ruterana, P., Monnet, I., Bluet, J., M. Bru-Chevallier, C. (2013). Journal of Optoelectronics and Advanced Materials, 15 (May-June2013), 471–474.
[15] Fonash, S. J. (1983). Journal of Applied Physics, 54(4), 1966–1975. https://doi.org/10.1063/1.332251